IOP Publishing Smart Materials and Structures
Smart Mater. Struct. 23 (2014) 045007 (11pp) doi:10.1088/0964-1726/23/4/045007

Shape memory polymer hexachiral auxetic structures with tunable stiffness

Jonathan Rossiter[1], Kazuto Takashima[2], Fabrizio Scarpa[3], Peter Walters[4] and Toshiharu Mukai[5]

[1] Department of Engineering Mathematics, University of Bristol, Bristol BS8 1UB, UK
[2] Graduate School of Life Science and Systems Engineering, Kyushu Institute of Technology, 2-4 Hibikino, Wakamatsu-ku, Kitakyushu 808-0196, Japan
[3] Department of Aerospace Engineering, University of Bristol, Bristol BS8 1TR, UK
[4] Centre for Fine Print Research, University of the West of England, Bristol BS3 2JT, UK
[5] Innovation Center, RIKEN, 2271-130 Anagahora, Shimoshidami, Moriyama-ku, Nagoya 463-0003, Japan

E-mail: Jonathan.Rossiter@bris.ac.uk

Received 21 September 2013, revised 23 December 2013
Accepted for publication 9 January 2014
Published 28 February 2014

Abstract
Planar auxetic structures have the potential to impact on a wide range of applications from deployable and morphing structures to space-filling composite and medical treatments. The ability to fabricate auxetics from smart materials greatly enhances this facility by building in controllable actuation and deployment. A smart auxetic device can be compressed and fixed into a storage state. When deployment is required the device can be appropriately stimulated and the stored elastic energy is released, resulting in a marked structural expansion. Instead of using a conventional external actuator to drive deployment the material is made to undergo phase transition where one stimulus (e.g. heat) initiates a mechanical response. Here we show how smart material auxetics can be realized using a thermally responsive shape memory polymer composites. We show how a shape memory polymer auxetic hexachiral structure can be tailored to provide a tunable stiffness response in its fully deployed state by varying the angle of inter-hub connections, and yet is still able to undergo thermally stimulated deployment.

Keywords: auxetic, shape memory polymer, deployable structures, actuator

(Some figures may appear in colour only in the online journal)

1. Introduction

Deployable structures are structures which can be transported in a compressed (e.g. low volume or low surface area) state and can then be controllably expanded to their deployed (e.g. high volume or high surface area) state when they reach their site of deployment (Pellegrino 2002). They are in great demand from the fields of engineering, space exploration (Puig *et al* 2010) and medicine (Kuribayashi *et al* 2006). For example, a deployable antenna can be packaged into a small volume at ground level and then transported into space where it is readily expanded into a large three-dimensional structure. The mean density of the expanded structure may be many orders of magnitude less than that of the compressed structure and this greatly reduces costs of transporting large structures into space. In the medical field a stent device can be compressed into a small enough volume so it can be injected into a patient. When appropriately stimulated it expands to a much larger size thereby restoring crucial blood flow in a vein or artery.

In conventional deployable structures the deployment process is typically driven by external electromechanical means such as motors, solenoids or through remote mechanical coupling such as cables (Puig *et al* 2010). Although these

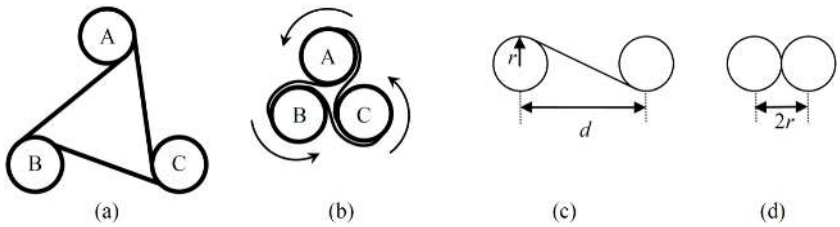

Figure 1. Contraction of chiral structures; (a) expanded and (b) compressed triangular element, (c) a single structural element at maximum extension and (d) at maximum contraction.

external deployment methods are effective there can be a significant cost in complexity, weight and transport where the deployment drive must also be transported to the site of deployment, used once, and thereafter left unused. Smart materials offer the solution to this problem by potentially providing a dual role of structural element (i.e. the deployable structure itself) and the internal deployment drive mechanism. Smart materials are materials which exhibit some measurable response to an external stimulus. Many smart materials have been developed which couple a wide variety of physical properties. For example shape memory alloys (Hassan *et al* 2008) and shape memory polymers (Bogue 2009) show a thermo-mechanical coupling, while electroactive polymers exhibit electro-mechanical coupling (Bar-Cohen 2004, Carpi and Smela 2009). Shape memory polymers are particularly attractive to developers of novel deployable structures because they combine the two important properties of zero-cost mechanical energy storage and a controllable one-way actuation. In contrast to shape memory polymers which can be formed into complex and multi-modal 3D structures through rapid prototyping methods or by casting in 3D moulds, shape memory alloys are typically formed in sheet and wire configurations which make them less suitable for many deployable structures. For complex structures shape memory alloys need to be bonded to separate components, resulting in a slower and more complex fabrication process, and regions of mechanical weakness (Hassan *et al* 2004). Additionally, shape memory polymers have much lower densities (typically 1/10 that of shape memory alloys) and generate much higher strains (up to 400% versus a maximum of 7% for shape memory alloys).

Many structural designs are amenable for use in deployable structures. These extend from simple radially expanding mechanisms (Conn and Rossiter 2010) to complete 3D folded origami structures (Furuya and Masuoka 2004). One important class of structure that is particularly suitable for deployable structures is that of auxetic structures (Evans and Alderson 2000). Auxetic structures are those that exhibit a negative Poisson's ratio, that is, when positive strain is introduced along one axis, the material shows positive strain along the directions normal to the applied strain. This is in contrast to conventional, non-auxetic, materials where positive strain in any axis must be counteracted by coupled negative strain in one or more other axis. The unusual deformation mechanism associated with auxeticity (expansion in all directions when pulled along one), has been used in the past as a way to develop structures and solids with shape-morphing capabilities. Examples are honeycombs with centresymmetric structures made from shape memory alloy ligaments (Hassan *et al* 2004, 2009), foams doped with magnetorheological fluids (Scarpa and Smith 2004, Bullogh and Scarpa 2005), rotating-unit structures with magnetic inserts (Grima *et al* 2013), auxetic plates exploiting mechanical instabilities in circular perforations (Shim *et al* 2013).

The natural extension of the basic properties of auxetic materials is that by applying a force in only one axis a deployable structure can be expanded from its stored, low volume, state to its deployed, high volume state. Since, in the minimal case, only one actuator is required to control the whole deployment process the structures can be transported with reduced cost. The disadvantage of this approach is that an external actuator is still required. A far better approach is for the auxetic structure to be fabricated from smart materials such as those described above. In such a case the auxetic structure can 'actuate itself' and deployment can be achieved with minimal cost and complexity.

In this paper we present shape memory polymer (SMP) hexachiral auxetic structures. These are auxetic structures fabricated from planar shape memory polymers. We show how these structures can be designed and fabricated and how they can be exploited as deployable structures through simple thermal cycling. We then show how their structures can be tuned for stiffness by varying chiral interconnections. These structures show highly effective self-deployment and offer the possibility of rapid fabrication of customizable deployable structures for a wide variety of applications.

2. Chiral auxetics

Although some materials naturally exhibit auxetic behaviour (Baughman *et al* 1998) it is the deployable characteristics of auxetic structures that we focus on in this research. Such structures can be fabricated from non-auxetic materials, making them suitable for a wide range of practical applications. One important class of auxetic structure is that of chiral auxetics. These structures are typically planar arrangements of finite-radius vertices connected by tangentially connected beams. Figure 1(a) shows an example of the tangential beam connections of a typical 3-vertex substructure from a hexachiral auxetic. The various chiral configurations and their auxetic characteristics have been investigated predominantly with respect to externally forced deformation (Evans and Alderson 2000, Prall and Lakes 1996, Abramovitch *et al* 2010, Alderson *et al* 2010). Although chiral structures can be

readily used for static structural and space-filling applications (Bettini *et al* 2010, Martin *et al* 2008), they also have great potential as active deployable structures. In such cases the chiral auxetic structure is transported from the fabrication point in a compressed form to the deployment location whereupon it is expanded to its deployed state. Due to the structural auxetic property (where expansion in two or more axes are mechanically linked) in many cases only one external actuator may be required. Instead of using an external actuator Hassan *et al* (2008) presented the first example of an active chiral auxetic, a hexachiral structure where connecting beams were made from shape-memory alloys. As the structure was heated the shape memory alloy beams transitioned from their programmed curled shape (illustrated by figure 1(b)) into straight beams (as in figure 1(a)), resulting in a significant overall expansion. This showed the potential of smart hexachiral auxetics to act as active mechanical structural elements for active space-filling and for structure deployment, for example in space applications, where no external actuators are needed (Jacobs *et al* 2012). The use of shape memory alloys however adds significant design and fabrication complexity. The shape memory polymer structures presented in this study largely overcome such limitations.

The transition of a smart chiral auxetic from compressed structure to fully deployed structure requires a measure of expansion capability. Here we define the linear expansion ratio as the ratio of the inter-centre distance between two adjacent vertices in expanded and compressed states. Figure 1(c) shows the maximum expansion and figure 1(d) shows fully compressed state where the thickness of the connecting beam is considered negligible. The linear expansion ratio here is $d/2r$, or $(l^2-4r^2)^{1/2}/2r$, where l is the length of the connecting beam. Where thickness w of beam is finite, this must be taken into account. This yields the mean number of rod thicknesses wrapped around each vertex as it winds up as $n = lm/4\pi r$ and the mean inter-centre distance at maximum compression as $2r + (2n+1)w$, where m is the number of rods connected to each hub. In the hexachiral structures presented here $m = 6$ and $n = 3l/2\pi r$. The maximum expansion ratio therefore becomes

$$R = \frac{d}{2r + (2n+1)w} = \frac{(l^2-4r^2)^{\frac{1}{2}}}{2r + (2n+1)w}. \qquad (1)$$

Additionally we define the area expansion ratio as the ratio of area of the triangle defined by the hub centres in the expanded triangular element in figure 1(a) and the compressed element in figure 1(b).

It is clear from figure 1(a) that imposition of an external compressive force on the expanded structure will cause the connecting beams to experience a combination of axial and bending forces. This will result in buckling of the beams into the characteristic second order 's' buckled beam shape in figure 1(b). Although control of structural stiffness is set at manufacture and is defined by parameters r, d, l, and the material properties of the connecting beams, behaviour under compressive loading always follows a similar shaped path through the stress–strain graph. More sophisticated control of expansion and structural stiffness can be achieved by employing materials such as shape memory polymers for the interconnecting beams.

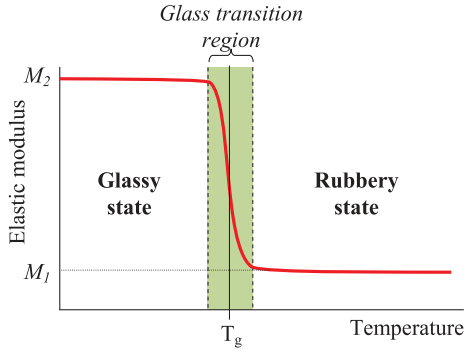

Figure 2. Typical glass transition behaviour in a single-shape memory polymer.

3. Shape memory polymer auxetics

3.1. Shape memory polymers

Shape memory polymers have responsive properties that set them apart from other plastic materials (Bogue 2009, Liu *et al* 2007). They are in demand from engineering and medicine because of their functional behaviour (Baer *et al* 2007, Sokolowski *et al* 2007). When appropriately stimulated a shape memory polymer (SMP) will undergo a change in elastic modulus. This typically occurs in a narrow range of stimulation. The majority of SMPs are thermo-responsive, that is, they respond to temperature change, although some light-responsive SMPs have been developed (Lendlein *et al* 2005). In similarity with other plastics these SMPs change their modulus around a glass transition temperature T_g. When the temperature T of the SMP is below T_g the material is in its high modulus state, often referred to as the glassy state. When the temperature of the SMP rises above T_g the material markedly softens and enters a low modulus state, often referred to as the rubbery state. This is illustrated in figure 2 which shows the change in modulus in response to temperature change. In marked contrast to other plastics, however, the SMP can store and controllably release mechanical energy. This characteristic is especially important for deployable structures where the stored mechanical energy can be released and coupled to drive the deployment mechanism. Figure 3(a) shows the typical cycle of stress, strain and temperature of a thermally stimulated shape memory polymer. The SMP with starting strain ε_0 is initially heated from below T_g to programming temperature T_p with no applied stress (A–B). A stress is then applied, resulting in consequential strain induction (B–C). The SMP is held at this constant stress as it is cooled to below T_g (C–D), and then the stress is removed (D–E). At this point the SMP is rigid and mechanical energy has been stored in the form of fixed strain ε. Subsequent heating without any applied stress to recovery temperature $T_r = T_p$ will release the stored energy and strain will be recovered (E–B). Cooling to below T_g returns the SMP to a state identical to the starting state (B–A). Note that, depending on the SMP, and how close it is to the ideal material, not all strain is recovered (i.e. $\varepsilon_r \neq \varepsilon_0$) and shape recovery may require heating above programming temperature, i.e. $T_r > T_p$, yielding the more

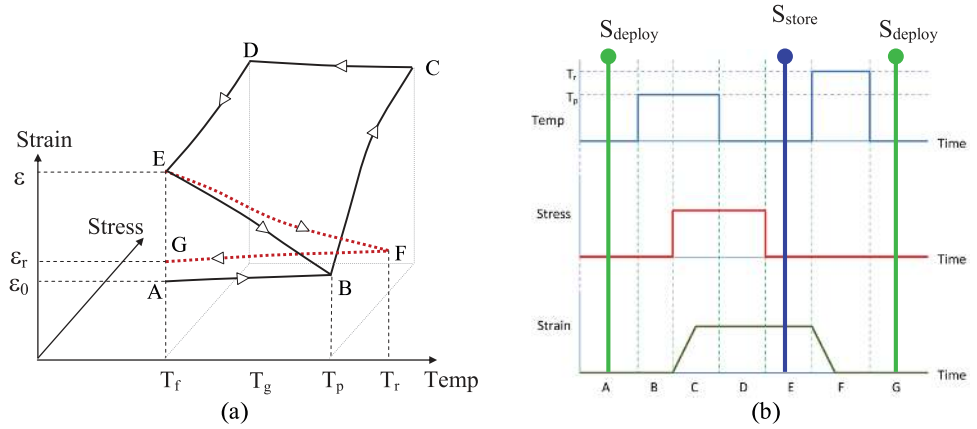

Figure 3. (a) Typical shape memory polymer cycle, (b) time domain storage, transportation and deployment cycle.

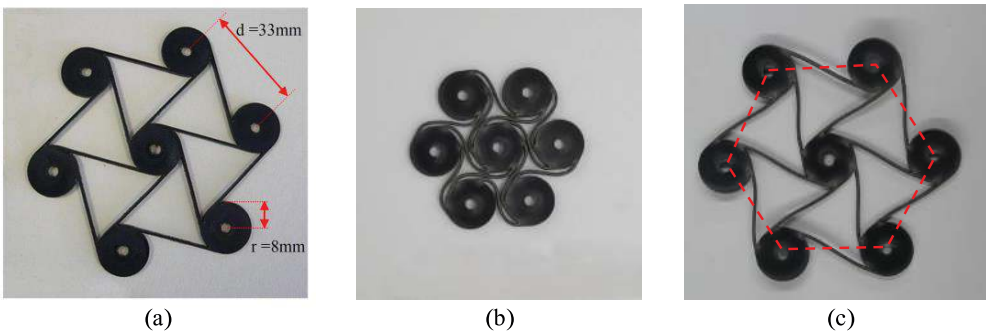

Figure 4. (a) As-fabricated deployed state of laser cut SMP hexachiral auxetic, (b) compressed storage state, (c) deployed structure after shape recovery.

realistic recovery path E–F–G. Figure 3(b) shows a temporal plot of the typical SMP cycle in terms of individual parameters of temperature, stress and strain. Here we can clearly see that the as-manufactured state is the full-sized deployed shape (S_{deploy}) and this is transitioned through the first half of the SMP cycle into a compressed storage state (S_{store}) for transport. When deployment is required the second half of the cycle is processed and deployed shape (S_{deploy}) is recovered. Note that only a simple thermal stimulus is required on-site to deploy the structure (F).

It is worth noting that shape memory effects have been observed in auxetic foams (Bianchi *et al* 2010a), leading to the production of converted specimens which, after the shape memory cycling, show enhanced mechanical and energy dissipation properties (Grima *et al* 2009, Bianchi *et al* 2010b). The attraction of exploiting shape memory polymers for deployable auxetic structures includes: easy fabrication of complex homogeneous structures; simple deployment by a single stimulus; high potential for fabrication into 3D deployable structures.

3.2. Shape memory polymer chiral elements

Chiral deployable structures have the potential to be fabricated from shape memory polymers through many routes including moulding, 3D printing and laser cutting of sheet material. In Rossiter *et al* (2012) the authors first proposed a shape memory polymer deployable structure. To demonstrate their potential a sheet of 1.75 mm thick Veritex shape memory polymer composite (Cornerstone Research Group) was laser cut into the full-sized deployment structure as shown in figure 4(a). Here the full 7-hub hexachiral element was fabricated in one pass. Note that dimensions were not optimized to match the characteristics of the material. Rod thickness is approximately 1 mm. The SMP hexachiral structure was then heated above the glass transition temperature of $T_g = 62$ °C and compressed by hand into the storage shape and cooled to fix the stored strain energy (figure 4(b)). This compressed structure was mounted on its central hub in a bath of water and slowly heated. The structure expanded when the temperature exceeded T_g and the deployed shape in figure 4(c) was recovered. This represents a linear expansion ratio of 1.5 and an area expansion ratio of 2.35. By (1) the maximum expansion ratio for a zero-width rod (i.e. $w = 0$) in this configuration is 2.06 and for a 1 mm thick rod is 1.54.

To further illustrate the potential of SMP hexachiral auxetics figure 5 shows the relative density of the structure as the SMP hexachiral was heated. Here relative density is defined as the ratio of the expanded area and the non-expanded area, where area is defined by the hexagon formed by the

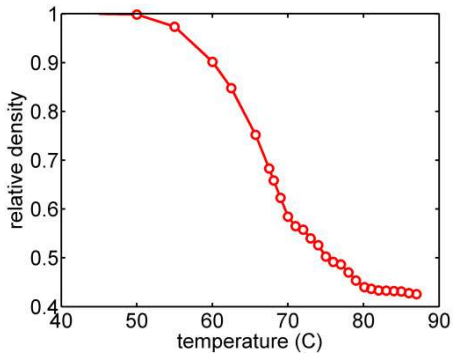

Figure 5. Relative density of the SMP hexachiral structure with increasing temperature.

straight-line connection of the outside six hubs, as shown in figure 4(c). This graph also shows that most stored energy is released around the glass transition temperature T_g, but that some stored energy is released over a wide range of temperatures from approximately 50 °C to approximately 80 °C. The sharpness of the transition shown in figure 2, and hence the sharpness of the energy release shown in figure 5 is dependent on the thermo-mechanical characteristics of the specific shape memory polymer used.

In a further demonstration the three-hub SMP auxetic element in figure 6(d) was fabricated from three strips of polynorbornene shape memory polymer (70 mm × 3 mm × 0.5 mm, $T_g = 35$ °C) bonded into 10 mm diameter acrylic hubs. Polynorbornene was used here in place of the Veritex composite in figure 4 due to its thinness, lower T_g and lower modulus in its rubbery state, permitting the easy and tight winding of the auxetic element into its storage state. The structure was heated to above T_g and compressed by hand to storage shape as shown in figure 6(a) and cooled to below T_g to fix the shape. The structure was then placed in a bath of hot water (approx. 55 °C) and observed to self-expand from its storage shape to its original deployment state. Here the relatively long length of the interconnecting rods with respect to hub radius yields a much higher linear expansion rate of 5.7 and area expansion ratio of 53.3. From (1) the maximum theoretical linear expansion ratio for this configuration with zero rod thickness is 6.5. For a rod thickness of 0.5 mm maximum linear expansion is 3.9. Note that the linear expansion of 5.7 measured here is for the triangular shape in figure 6(d) where four rods connections per hub needed for the full hexachiral are missing, which results in a consequently tighter shape when contracted and larger linear and area expansion ratios.

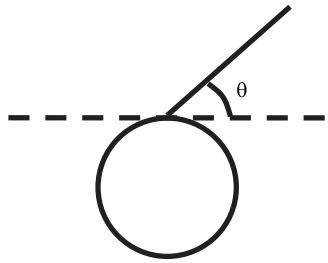

Figure 7. Rod–hub connection at angle θ.

4. Tunable stiffness

The two examples in figures 4 and 6 clearly demonstrate the self-deployment capabilities of SMP chiral auxetics. Note that the two structures are fundamentally different in the inter-hub connections. In figure 4 hubs are connected by rods that are connected at the tangent to the external circumference of the hubs. In contrast the rods in figure 6 are connected radially. This difference will result in different behaviours when the deployed structures are exposed to external compressive forces. Compression of the tangentially connected figure 4 will result in induced rotation of the external and internal hubs as defined by the direction of tangential connectivity of the rods and the consequent resolution of compressive forces into torsion (Spadoni and Ruzzene 2012). In effect the structure will start to 'wind-up' under external compression. Compression of the radially connected figure 6 will not induce such a pre-defined hub rotation or wind-up due to the symmetry of the rod connections.

We can explore the difference between these two structures through the parameter θ, the angle of connecting rod with respect to the tangent of the circumference of the hubs, as illustrated in figure 7, in the range $\theta \in [0, \pi/2]$ rad. If we construct a hexachiral structure where all rods are connected with angle $\theta = 0$ we obtain the structure in figure 8(a), corresponding to the conventional hexachiral auxetic structure. If, on the other hand, we construct a hexachiral structure with $\theta = \pi/2$ we obtain the radially connected structure in figure 8(b). Here the diameter of the hubs contribute to the larger area coverage of this structure than for the case where $\theta = 0$.

The attraction of varying θ is that it will have impact not only on the area coverage of the structure but also on its deployed strength and its behaviour during expansion. The deployed strength of the $\theta = 0$ structure will be less than that of

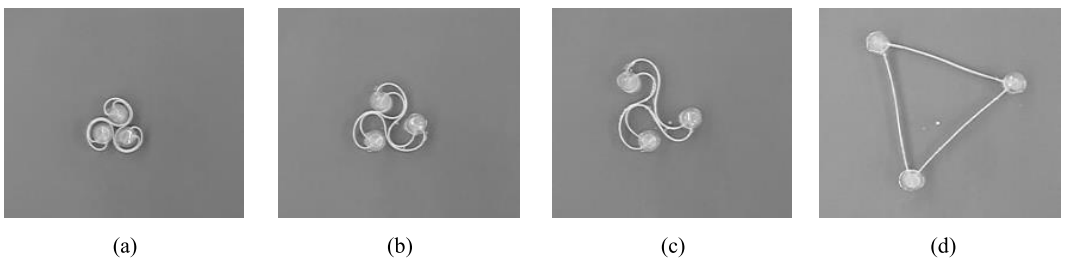

Figure 6. Recovery of deployment shape upon immersion in warm water. Frames (a)–(c) are 1 s apart. Frame (d) is 24 s later. (a) $t = 1$ s. (b) $t = 2$ s. (c) $t = 3$ s. (d) $t = 27$ s.

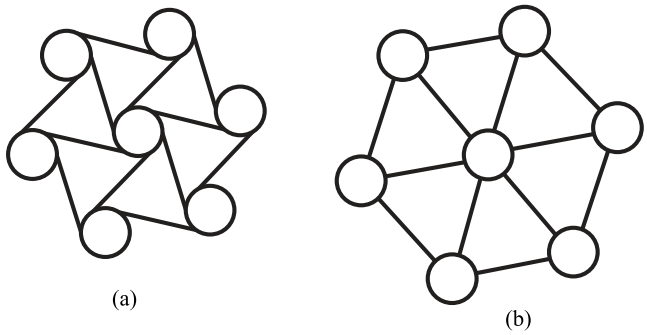

Figure 8. Deployed state for (a) $\theta = 0$, and (b) $\theta = \pi/2$, hexachiral structures.

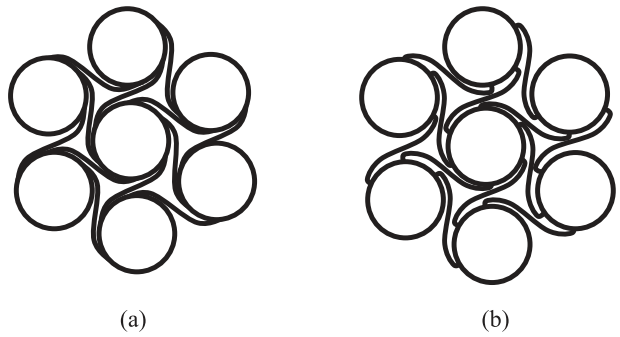

Figure 9. Storage states for (a) $\theta = 0$, and (b) $\theta = \pi/2$, hexachiral structures.

the $\theta = \pi/2$ structure because it resolves external forces into internal torsion distributed across the structure. This yields a classic auxetic behaviour upon compression. The deployed strength of the $\theta = \pi/2$ structure, on the other hand, is the result of the radially connected rods which form a network of axially compressed Euler beams. As such these beams will be subject to classic Euler buckling behaviour with a characteristic high initial strength up to critical compression after which strength falls rapidly.

Another important consequence of varying θ is on the compressed, storage state of the auxetic structure, and the local stresses imposed on the materials. For example, where $\theta = 0$ the compressed auxetic will resemble the shape in figure 9(a). Here the tangentially connected structure can be compressed tightly because the radius of curvature of the rod at the hub connections is large and bending stresses will be relatively small. In contrast, when $\theta = \pi/2$ the compressed radially-connected structure will resemble the shape in figure 9(b). Here compression imposes a small radius of curvature on the rod at the hub connections, with corresponding high bending stresses. The flip-side of this is that, when the structure is deployed the high local bending stresses in the $\theta = \pi/2$ structure can be expected to result in higher deployment moments, depending on the materials being used.

Importantly, while the $\theta = 0$ structure (figures 8(a) and 9(a)) behaves as an auxetic in both expansion and compression, the $\theta = \pi/2$ structure (figures 8(b) and 9(b)) is auxetic in expansion but not necessarily in compression. Bi-directional auxetic behaviour will therefore be present when $0 \leq \theta < \pi/2$ and uni-directional auxetic behaviour is present when $\theta = \pi/2$. Figure 10 illustrates the expanded $\theta = \pi/2$ structure when subsequently loaded. For clarity only two of the six radial rods and three hubs are shown. Each rod under load will undergo Euler buckling, the direction of deflection of which is non-deterministic. Figure 10(a) shows that if deflection direction is the same for all rods (with respect to rotation about the central hub) the central hub will undergo rotational wind-up. When rod defection directions are opposite, this will counteract rotation of the central hub and there will be no wind-up (figure 10(b)). For the single n-chiral element we would expect the wind-up case, when all rods buckle in the same direction, to occur with a low probability of 2^{1-n}. In reality we might expect a uniform distribution of the two buckling directions across a larger structure, resulting in a range of local cases from high structural strength to lower strength wind up. Although analysis of the complex deformation under load of these structures is beyond the scope of this paper, recent work by Yang *et al* (2013) has however shown that sandwich structures with re-entrant auxetic cores under similarly large deformations exhibited more homogeneous deflection and bending in comparison to conventional core designs. This suggests the macro-scale properties of these structures will have advantages over competing designs.

To investigate the potential of varying θ for these chiral auxetic structures we now consider the compression and expansion of structures of hubs and rods, which can then be extrapolated to the full auxetic structure.

5. Experimental results

Self-expanding elementary structures with varying θ were fabricated and tested using rods of shape memory polymer. Hubs were fabricated from rigid ABS plastic.

5.1. Compression of deployed structures

We consider the two elementary components in figure 11 where figure 11(a) shows the $\theta = \pi/2$ rod–hub connection and figure 11(b) shows the $\theta = 0$ connection. The dimensions of the shape memory polymer connecting rod are 20 mm × 120 mm × 2 mm. The hubs had external radius 34 mm. The SMP material was Veritex with glass transition temp $T_g = 62$ °C. Figure 12 shows the experimental setup used to evaluate deformation under axial compression. The structures in figure 11 were each mounted on free-to-rotate

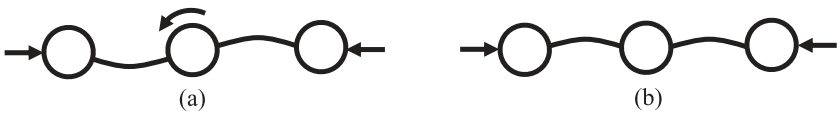

Figure 10. (a) Wind-up induced by rods buckling in same direction, and (b) no wind-up where rods buckle in opposite directions.

(a) (b)

Figure 11. Elementary components composed of a single shape memory polymer rod (120 mm length) and plastic hub for the two cases; (a) $\theta = \pi/2$, (b) $\theta = 0$.

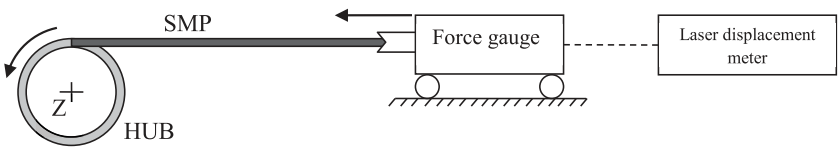

Figure 12. Experimental setup for axial loading.

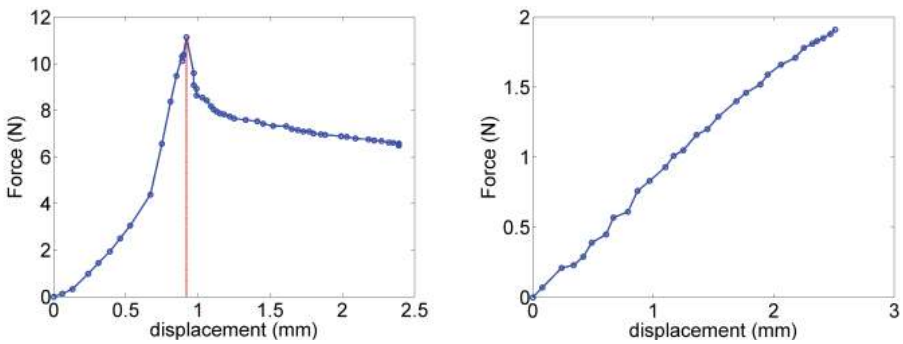

(a) (b)

Figure 13. Force–displacement graphs as each of the elementary structures is axially loaded. (a) $\theta = \pi/2$, (b) $\theta = 0$.

bearing at Z. A metal rod with a 'v' shaped cut-out was attached to a force gauge (AND 4932A-50N) mounted on a moveable stage. The stage was moved forward at a slow rate (approx. 0.28 μm s^{-1}) such that the gradually increasing axial loading was applied to the SMP beam. A laser displacement meter (Keyence LC-2400) simultaneously measured displacement of the stage. Temperature was kept at room temperature (approx. 28 °C), well below the glass transition temperature T_g of Veritex. To capture behaviour around the deployment point the stage movement range was limited to 2.5 mm, sufficient to clearly differentiate the mechanical behaviour of the two structures.

Figure 13 shows the typical stress–strain graph for the $\theta = \pi/2$ (figure 13(a)) and $\theta = 0$ (figure 13(b)) cases. Figure 13(a) shows an exponential increase in stiffness as axial load is applied, up to the critical load point of 11 N at 0.92 mm displacement. After this point the beam buckled and subsequent increases in strain resulted in reduced stress and the beam bend outward into a pronounced curve. Figure 13(b) shows no critical loading point since buckling is initiated at the start of loading. This is due to the induced bending at the rod–hub interface and the rotating base. Here stiffness is much more linear then for the $\theta = \pi/2$ case and compressive force is much less, even at maximum displacement. These two graphs demonstrate the two extremes of stiffness behaviour that can be incorporated into the proposed shape memory polymer auxetic structures with variable rod–hub angle. Figure 14 shows deformation of the two cases for axial strain of 2.5 mm. Note the greater rod curvature for the $\theta = \pi/2$ case.

These results are confirmed by 2D FEA analysis as shown in figures 15 and 16. In figure 15 ($\theta = \pi/2$) the rotational hub is simulated by a rigid rod of length the same as the hub radius that is free to rotate at one end (point P in figure 15) and fixed axially to the SMP material at the other end (point Q). In figure 16 ($\theta = 0$) the hub is simulated by the same rigid rod but now fixed at right angles to the SMP beam (point R). In both cases axial compression is constrained to the X axis only and beam deflection is constrained to the XY plane. A fixed

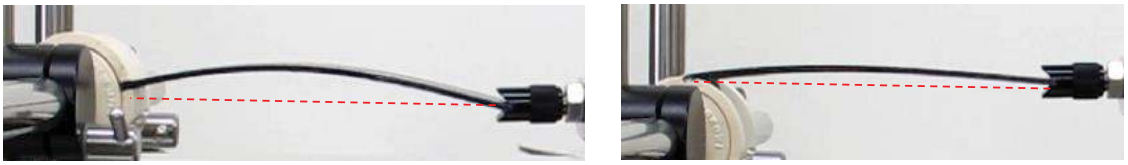

(a) (b)

Figure 14. Rod deflection at 2.5 mm displacement (a) $\theta = \pi/2$, (b) $\theta = 0$.

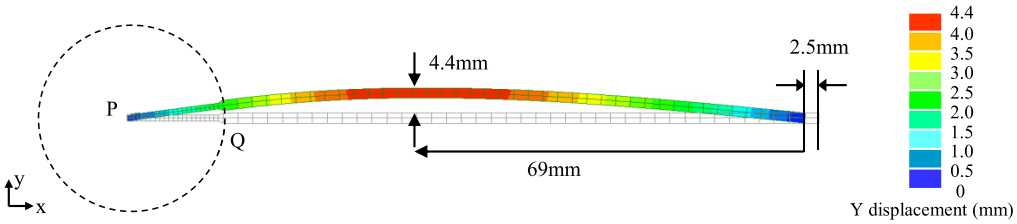

Figure 15. FEA model of radial connection ($\theta = \pi/2$) showing buckling under axial strain of 2.5 mm.

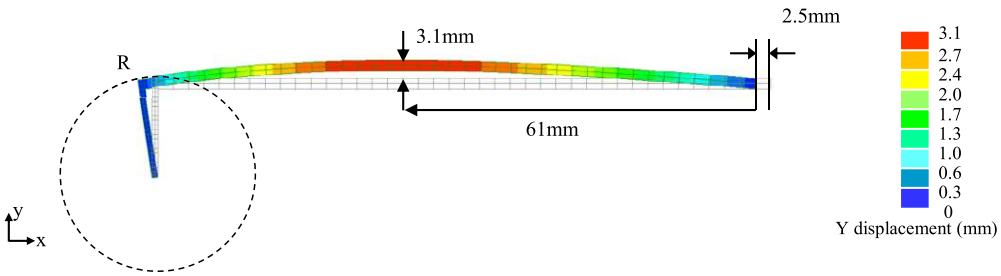

Figure 16. FEA model of tangent connection ($\theta = 0$) showing buckling under axial strain of 2.5 mm.

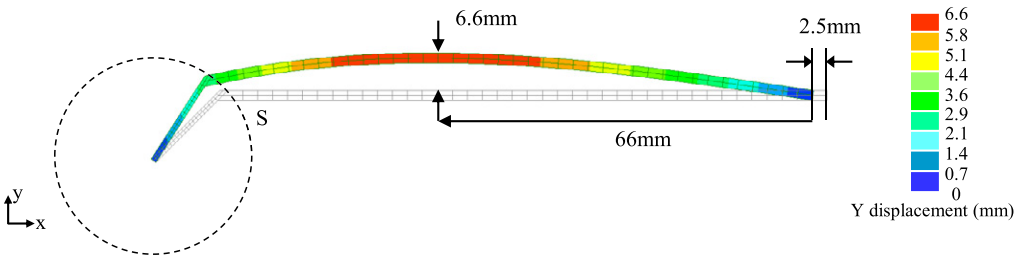

Figure 17. FEA model of tangent connection ($\theta = \pi/4$) showing buckling under axial strain of 2.5 mm.

strain of 2.5 mm is applied to the tips of both rods and the model is solved for beam deflection. For the $\theta = \pi/2$ case a very small asymmetry is implemented at mounting point P to initiate buckling and to bias the beam to upward deflection.

Note the slightly different buckling shapes, as indicated by the point of maximum vertical displacement (measured from the right end of the rod) of 69 mm for radially connected rod (4.4 mm deflection) in figure 15 and 61 mm for tangential connected rod (3.1 mm deflection) in figure 16.

As the angle θ is varied from $\theta = 0$ to $\theta = \pi/2$ the strength of the structure increases, yielding the primary parameter by which structural strength can be tuned. However the deflection of the rod in the y axis reaches a maximum within the interval $0 < \theta < \pi/2$. This is illustrated in figure 17 for the $\theta = \pi/4$ case where deflection of the beam from starting state (6.6 mm) is larger than both the $\theta = \pi/2$ and the $\theta = 0$ cases. This is due to the larger rotation of point S around the circumference of the hub, and hence the larger displacement in the y axis. For the $\theta = \pi/2$ case the axial compression constrains rotation and vertical displacement of point Q, and for the $\theta = 0$ case negligible vertical displacement of point R is observed during small angles of rotation. Future work will examine the relationship between θ and structural strength in more detail.

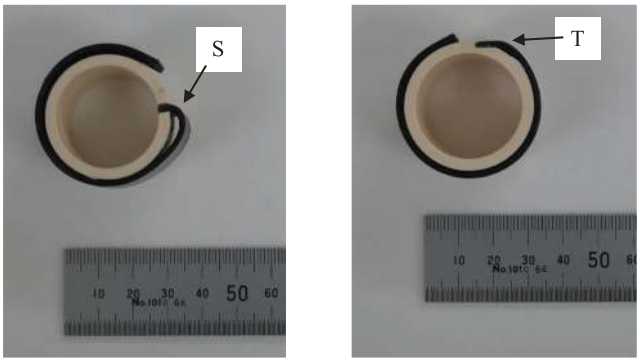

Figure 18. Shape programmed elementary structures, (a) $\theta = \pi/2$, (b) $\theta = 0$.

5.2. Shape memory deployment

The deployment of a pre-compressed shape memory polymer auxetic structure involves applying sufficient thermal stimulation to raise the temperature above T_g. The structure will then transition smoothly from the storage state to the deployed state. The tunable stiffness proposed above involves differences in the hub and rod interconnections. We would expect such geometric differences to result in differences in the rate, and possibly the extent, of deployment. To investigate the effects on deployment of varying θ as described above, the two experimental structures (one with $\theta = \pi/2$ and one with $\theta = 0$) with plastic hubs and SMP rods as in figure 11 were heated in hot water above T_g and the SMP rods were hand wound tightly around the hubs. These were then dipped in cold water below T_g to fix the shapes. Figure 18 shows the two wound structures. Note the large local bending in the $\theta = \pi/2$ case (figure 18(a), point S) where the rod enters the hub, and the much smoother bending in the $\theta = 0$ case (figure 18(b), point T). This closely matches the compressed states of the two auxetic structures proposed in figure 9. It is also clear that this deformation limits how close hubs can be compressed in the storage state and hence will negatively affect the deployment ratio.

These structures were then mounted at their hubs and lowered into hot water above T_g. The SMP beams were thereby free to return to their pre-compression shapes. Figure 19 shows shape recovery of the programmed structures in figure 18. Here SMP beam profiles were extracted from 17 video frames at 2 s intervals. Dashed circles show position and size of the central hubs. Angle φ is defined as angle between two line connecting the position of the end point of the beam and the centre of the hub and the line connecting the starting position of the end point and the hub (as shown in figure 19(a)). Note how the radially-fixed structure (figure 19(a)) recovers its original flat shape faster (by approx. 4 frames or 8 s) than the tangent-fixed structure (figure 19(b)).

Clearly the thermal energy input into the proposed auxetic SMP structures will need to be removed in order to reduce its temperature and fix the structure (i.e. $T < T_g$) and this process will be dependent on the specific heat capacity of the polymer (typically of the order of 1–2 J g^{-1} K^{-1} (Cho *et al* 2005)), its coefficient of thermal expansion (Lim 2011) and the distribution of thermal stresses (Lim 2013, Maruszewski *et al* 2013). These characteristics will determine the heating and cooling times and hence the maximum frequency of thermal cycling.

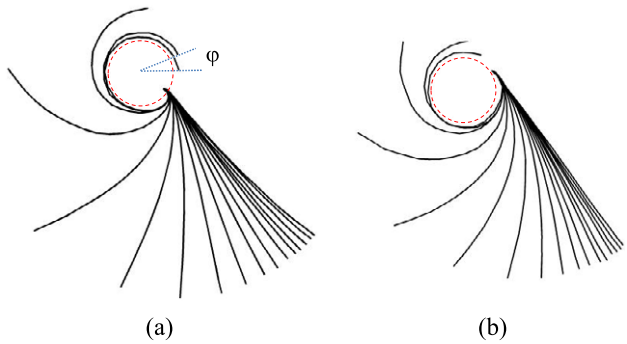

Figure 19. Shape recovery of elementary structures, (a) $\theta = \pi/2$, (b) $\theta = 0$.

Figure 20 shows the angle and angular velocity of the SMP rods during the shape recovery (i.e. deployment) process. Although the two structures have relatively similar deployment profiles it is clear that the $\theta = \pi/2$ case shows faster and larger deployment. This is attributed in large part to the release of stored energy in the tight bend of the hub–rod interface (S in figure 18(a)).

Note that internal stresses imposed by the anisotropic composite nature of the Veritex shape memory polymer result in recovery beyond the original flat shape, as shown in figure 19(a). Figure 21 shows magnified images of the two planar sides of the Veritex sheet. Note the difference in matrix weave and the presence of a smooth coating of Veriflex resin on the bottom surface (figure 21(a)). Such effects can be overcome by fabricating the polymer into a symmetric composite structure. On the other hand these stresses may be managed and exploited depending on the application. Note that in figure 14 the smooth surface is to the top and in figure 18 the smooth surface is to the outside.

Note also that these shape memory polymer auxetic structures can be reused and reprogrammed, or even re-moulded, for example after recovery of a deployed structure, but additional thermal and mechanical energy is required. This is impractical within many environments such as outer space. In these applications shape memory deployment is most likely to be single use only.

Depending on the polymer or composite used the auxetic structures can be scaled arbitrarily. For example, these SMP hexachiral structures have the potential to be exploited in large scale building projects as well as millimetre-scale stents. The limit in large scale structures is likely to be in the control and uniformity of thermal stimulation.

6. Conclusions

In this work we have presented novel shape memory auxetic deployable structures that need no external actuation mechanisms. Shape memory polymers are ideal for such

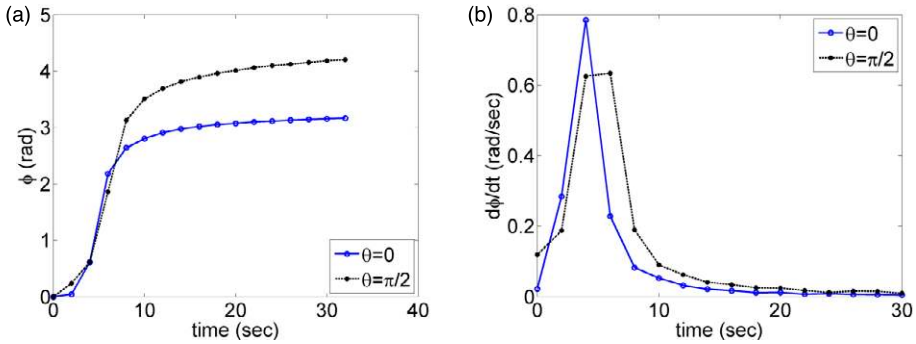

Figure 20. (a) Angle of SMP rods during shape recovery, and (b) angular velocity.

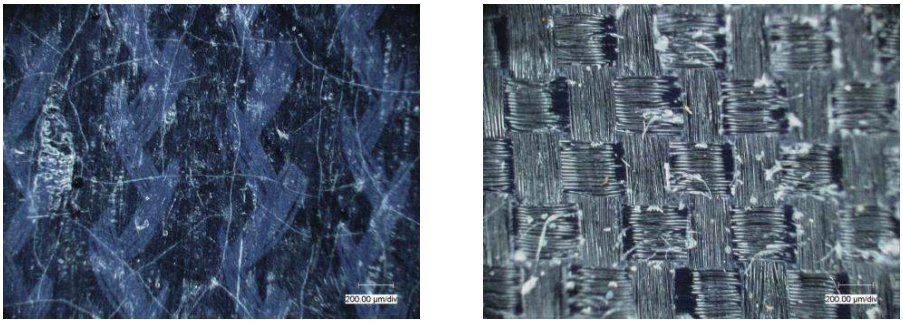

(a) (b)

Figure 21. Anisotropic structure of Veritex composite, (a) smooth bottom surface with diamond weave, and (b) rough top surface with square weave.

structures because of their robustness and low costs. They are also amenable to ready fabrication and shaping using simple and low-cost methods such as moulding and 3D rapid prototyping. We have shown that by changing the hub–rod angle θ the characteristics of the deployment process and the mechanical properties of the deployed structure can be tailored to meet the application. The two limit cases of radial connection ($\theta = \pi/2$) and the tangential connection ($\theta = 0$) were investigated and results show a large range in mechanical and deployment characteristics. Choice of θ also has an impact of the compactness of the storage structure and the size of deployed structure, which may have knock-on impact on transportation costs, for example in deployment of structures in outer space. The potential versatility of these self-actuating structures includes the option of employing different hub–rod angles for different hubs and the tuning of expansion so that a specific intermediate stiffness and expansion force is generated, for example to overcome mechanical resistance in an attached structure or material. Future work will further examine the structural properties of the deployed and storage states and will investigate the full range of fabrication methods and geometries that can further increase the applicability of these technologies.

Acknowledgments

This work was funded jointly by the UK Engineering and Physical Sciences Research Council (EPSRC) under grant EP/I032533/1 and through the EPSRC Building Global Engagements in Research programme.

References

Abramovitch H, Burgard M, Edery-Azulay L, Evans K E, Hoffmeister M, Miller W, Scarpa F, Smith C W and Tee K F 2010 Smart tetrachiral and hexachiral honeycomb: sensing and impact detection *Compos. Sci. Technol.* **70** 1072–9

Alderson A, Alderson K L, Chirima G, Ravirala N and Zied K M 2010 The in-plane linear elastic constants and out-of-plane bending of 3-coordinated ligament and cylinder-ligament honeycombs *Compos. Sci. Technol.* **70** 1034–41

Baer G, Wilson T S, Matthews D L and Maitland D J 2007 Shape-memory behavior of thermally stimulated polyurethane for medical applications *J. Appl. Polym. Sci.* **103** 3882–92

Bar-Cohen Y (ed) 2004 *Electroactive Polymer (EAP) Actuators as Artificial Muscles—Reality, Potential and Challenges* PM136, 2nd edn (Bellingham, WA: SPIE Press)

Baughman R H, Shacklette J M, Zakhidov A A and Stafstrom S 1998 Negative Poisson's ratios as a common feature of cubic metals *Nature* **1998** 362–5

Bettini P, Airoldi A, Sala G, Di Landro L, Ruzzene M and Spadoni A 2010 Composite chiral structures for morphing airfoils: numerical analyses and development of a manufacturing process *Composites* B **41** 133–47

Bianchi M, Scarpa F and Smith C W 2010a Shape memory behaviour in auxetic foams: mechanical properties *Acta Mater.* **58** 858–65

Bianchi M, Scarpa F, Smith C W and Whittell G R 2010b Physical and thermal effects on the shape memory behaviour of auxetic open cell foams *J. Mater. Sci.* **45** 341–7

Bogue R 2009 Shape-memory materials: a review of technology and applications *Assem. Autom.* **29** 214–9

Bullogh W A and Scarpa F 2005 Electrically controlled extension effects in soft solids *Int. J. Mod. Phys.* B **19** 1655–60

Carpi F and Smela E (ed) 2009 *Biomedical Applications of Electroactive Polymer Actuators* (New York: Wiley)

Cho J W, Kim J W, Jung Y C and Goo N S 2005 Electroactive shape-memory polyurethane composites incorporating carbon nanotubes *Macromol. Rapid Commun.* **26** 412–6

Conn A T and Rossiter J M 2010 Radially expanding mechanism for dielectric elastomers *Proc. SPIE* **7642** 1–11

Evans K E and Alderson A 2000 Auxetic materials: functional materials and structures from lateral thinking *Adv. Mater.* **12** 617–27

Furuya H and Masuoka T 2004 Concept of rotationally skew fold membrane for spinning solar sail *IAC: Proc. 55th International Astronautical Congress (IAC-04-I.1.05, Vancouver, Oct. 2004)* pp 1–5

Grima J N, Attard D, Gatt R and Cassar R N 2009 A novel process for the manufacture of auxetic foams and for their re-conversion to conventional form *Adv. Eng. Mater.* **11** 533–5

Grima J N, Caruana-Gauci R, Dudek M R, Wojciechowski K W and Gatt R 2013 Smart metamaterials with tunable auxetic and other properties *Smart Mater. Struct.* **22** 084016

Hassan M R, Scarpa F L and Mohamed N A 2004 Shape memory alloys honeycomb: design and properties *Proc. SPIE: Smart Struct. Mater.* **5387** 557–64

Hassan M R, Scarpa F and Mohamed N A 2009 In-plane tensile behavior of shape memory alloy honeycombs with positive and negative Poisson's ratio *J. Intell. Mater. Syst. Struct.* **20** 897–905

Hassan M R, Scarpa F, Ruzzene M and Mohammed N 2008 A smart shape memory alloy chiral honeycomb *Mater. Sci. Eng.* A **481/482** 654–7

Jacobs S, Coconnier C, DiMaio D, Scarpa F, Toso M and Martinez J 2012 Deployable auxetic shape memory alloy cellular antenna demonstrator: design, manufacturing and modal testing *Smart Mater. Struct.* **21** 75013–24

Kuribayashi K, Tsuchiya K, You Z, Tomus D, Umemoto M, Ito T and Sasaki M 2006 Self-deployable origami stent grafts as a biomedical application of Ni-rich TiNi shape memory alloy foil *Mater. Sci. Eng.* A **419** 131–7

Lendlein A, Jiang H, Junger O and Langer R 2005 Light-induced shape-memory polymers *Nature* **434** 879–82

Lim T-C 2011 Coefficient of thermal expansion of stacked auxetic and negative thermal expansion laminates *Phys. Status Solidi* b **248** 140–7

Lim T-C 2013 Thermal stresses in thin auxetic plates *J. Therm. Stresses* **36** 1131–40

Liu C, Qin H and Mather P T 2007 Review of progress in shape-memory polymers *J. Mater. Chem.* **17** 1543–58

Martin J, Heyder-Bruckner J-J, Remillat C, Scarpa F, Potter K and Ruzzene M 2008 The hexachiral prismatic wingbox concept *Phys. Status Solidi* b **245** 570–7

Maruszewski B T, Drzewiecki A and Starosta R 2013 Thermoelastic damping in an auxetic rectangular plate with thermal relaxation-free vibrations *Smart Mater. Struct.* **22** 084003

Pellegrino S (ed) 2002 *Deployable Structures, CISM International Centre for Mechanical Sciences* (Berlin: Springer)

Prall D and Lakes R 1996 Properties of a chiral honeycomb with a Poisson's ratio-1 *Int. J. Mech. Sci.* **39** 305

Puig L, Barton A and Rando N 2010 A review on large deployable structures for astrophysics missions *Acta Astronaut.* **67** 12–26

Rossiter J, Scarpa F, Takashima K and Walters P 2012 Design of a deployable structure with shape memory polymers *Proc. SPIE* **8342** 83420Y

Scarpa F and Smith F C 2004 Passive and MR fluid-coated auxetic PU foam—mechanical, acoustic, and electromagnetic properties *J. Intell. Mater. Syst. Struct.* **15** 973–9

Shim J, Shan S, Košmrlj A, Kang S H, Chen E R, Weaver J C and Bertoldi K 2013 Harnessing instabilities for design of soft reconfigurable auxetic/chiral materials *Soft Matter* **9** 8198–202

Sokolowski W, Metcalfe A, Hayashi S, Yahia L and Raymond J 2007 Medical applications of shape memory polymers *Biomed. Mater.* **2** S23–7

Spadoni A and Ruzzene M 2012 Elasto-static micropolar behavior of a chiral auxetic lattice *J. Mech. Phys. Solids* **60** 156–71

Yang L, Harrysson O, West H and Cormier D 2013 A comparison of bending properties for cellular core sandwich panels *Mater. Sci. Appl.* **4** 471–7